Article Identifier
DOI: 10.22032/dbt.58915
URN: urn:nbn:de:gbv:ilm1-2023isc-111:9

60th ILMENAU SCIENTIFIC COLLOQUIUM
Technische Universität Ilmenau, 4 – 8 September 2023
URN: urn:nbn:de:gbv:ilm1-2023isc:1

MOLECULAR DYNAMICS SIMULATION OF GALLIUM PHOSPHIDE ZINCBLENDE CUTTING MECHANISM

M.R.P.M. Tavares[1,2], D.A. Rolon[1], J. Kober[1], *S. Kühne[1], R. B. Schroeter[2], D. Oberschmidt[1]*

[1]Technische Universität Berlin, Department of Micro and Precision Devices (MFG), Germany
[2] Federal University of Santa Catarina, Laboratory of Precision Engineering (LMP), Brazil

ABSTRACT

Gallium Phosphide (GaP) has a low machinability, due to high tool wear and the need to induce a High-Pressure Phase Transformation (HPPT). HPPT changes GaP crystallographic structure from zincblende to β-tin. The latter is ductile and metastable, therefore, rather than be experimentally observably, must be simulated using atomistic methods. In this work, Classic Molecular Dynamics Simulations (CMDS) were used to analyse GaP HPPT and tool wear mechanisms during the cutting process. Diamond tools were modelled with 10 nm cutting edge radius, -20º and -10º rake angles, and -10º clearance angle. The simulations revealed that the main shear mechanism involved stacking faults, planar dislocations within the crystal structure, while HPPT had a limited role, being restricted to the deformation zone. A more significant surface crack and tool amorphization were observed for a rake angle -10º.

Index Terms - Gallium Phosphide, Machining, Molecular Dynamics Simulations, Vashishta potential, Semiconductor.

1. INTRODUCTION

New designs for optical elements can be achieved through materials with enhanced optical properties. For the visible (VIS) and near infrared (NIR) applications. The semiconductor gallium phosphide (GaP) from the group III-V has a good combination of refractive index, transmissibility, and mechanical properties [1–3]. Regardless of the advantageous designs that the combination of these properties propitiate, applications of GaP is mostly limited towards green LEDs [2]. For optical applications, GaP elements commonly demand polishing as a post-process to reach an optical quality surface. Such process leads to the formation of PH_3, which is toxic, due the contact with water [2,4]. Also, attempts to machine GaP with a monocrystalline diamond tool have led to surface quality appropriated for optical applications, however at cost of considerable tool wear [5]. In order to efficiently manufacture GaP, an in-depth understanding of the cutting mechanisms acting during the process can provide valuable information. Finite element methods (FEM) approaches are limited for describing atomic-scale transformations which is common in semiconductor from III-V group under cutting condition[6]. The issues are both from theoretical and practical order. From theoretical perspective, it is necessary to know in advance the chip morphology, and properties of all material phases. Additionally constitutive equations are not tested under the conditions imposed by the cutting. For instance, the plastic deformation rate involved in machining is usually higher than ones achievable by stress-strain or Split Hopkinson bar tests [7,8]. From practical perspective, the material separation demands a remeshing process increasing the total simulation time. Hence, since the cutting of brittle semiconductor, such as GaP, relay on High-

Pressure Phase Transformations (HPPT) and movement of dislocations, Classic Molecular Dynamics Simulations (CMDS) were chosen for modelling [9].
CMDS calculates a multi-body dynamic. Each body represents an atom, whose trajectory is obtained through the integration of Newton's equation of motion in time intervals in the order of femtoseconds. The integral process starts calculating the potential energy (U) for each atom. For that, potential energy function with a set of specific parameters for each material, known as force field [10–12] is required. As it happens for FEM constitutive equations, a material may have different force fields available in literature, and each one may be useful for a different application. This force fields are typically approximations of density functional theory (DFT) simulations or other *ab inito* methods, capable of describing the electronic interaction between atoms. Because of its atomic nature, CMDS can be useful for analyze crystallographic imperfections, such as cracks and dislocations. Additionally, if a force field allows, it is also possible to predict phase transformations [13].
Since even small quantities of matter may have trillions of atoms, models used in CMDS are typically on the nanometric scale and a total simulation can take a long time to run without some computational constrains and mathematical resources. During CMDS, each atom exerts a force in nearby atoms and the resultant force on each atom depends on all its neighbors. Ideally, all atoms in a system are neighbors, but in order to reduce the demanded processing power, only those within a specific range are considered. This specific range is known as cut-off and it is used to delimit a neighbor list for each atom, which represents the set of relevant atoms to be tracked for resultant force calculations. Each atom has its own neighbor list and each simulation has a way to determine when a list should be updated [10]. The update rate of the neighbor lists may be critical for the total simulation time and precision. Another resource is the periodic boundary, used to represent systems that are physically bigger. If one a boundary of a system is considered periodic in a specific direction; an image of the system is created in each side of that direction. As a result, atoms in opposed side of a periodic boundary can interact with each other. Finally, due the bond between timestep and a physical time, specific solutions for each problem might be used for speed up a simulation. For example, during machining simulations, the cutting speed is set as much higher than those applied in real machining processes, allowing the tool to move a significant distance in a feasible simulation time [14].
Post-process is also critical for CMDS. For example, crystallographic structures cannot be analyzed for large sets of atoms, therefore structure identification algorithms are required. One of them is the dislocation extraction algorithm (DXA) [15–17] from the OVITO® software. This one not only determine structures as well as Burge vectors. Another one is the Polyhedron Template Match (PTM) [18], capable of determine crystallographic structures faster than DXA. Since not all structures are trackable by each algorithm, additional post-processing tools are required, such as coordination analysis, which gives the number of neighbor atoms in a shell of each atom, the coordination number [19]. To calculate continuous mechanics variables, time e/or spatial average are required. For example, the temperature is calculated based on the average speed of an atoms in the 3 directions [9,20].
The use of CMDS to predict cutting mechanisms started on late 80's [21,22] focusing on metals and moved to semiconductors in the last decade [9,23]. The goal of the studies can be either the tool, the workpiece or both. If the tool is set to be infinitely rigid, no tool wear can be analyzed and the material behavior is studied, including phase transformations, how cracks are formed and the temperature during the cutting. When the tool wear is to be studied, abrasion, graphitization and amorphization a typically analyzed. Other mechanisms are reported in literature as well: diffusion [24] and chemical reaction [25].
For the present work, the cutting mechanisms of GaP in the direction [100] are investigated. The model used also allows tool wear analysis, which are studied as well alongside the impact of the tool geometry on the cutting.

2. TOOL MODELLING PROCESS

The tool was modelled firstly as a block. Atoms in the bases of the diamond lattice structure were set and, using the function *meshgrid* function from MATLAB®, a region in a block like shape was filled with atoms. After that, the block was shaped to become the tool in a sequence represented on *Figure 1*.

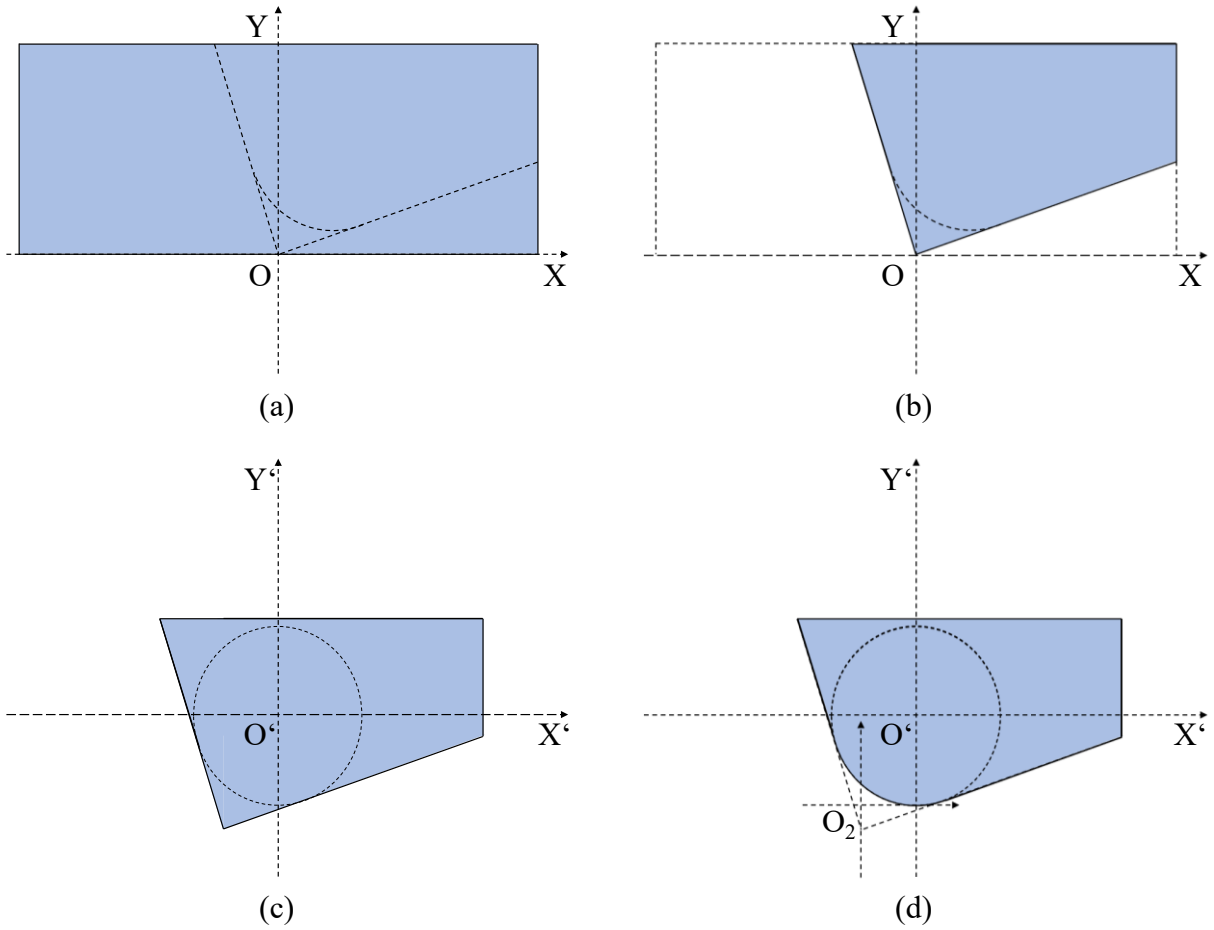

Figure 1 – Modelling sequence: (a) Block, (b) rake and clearance angles, (c) translation to the center of the tool cutting edge circle, and (c) round the tool cutting edge and defining a new origin O_2.

Between *Figure 1*(a) and (b) and once more between *Figure 1* (c) and (d), it was performed a cartisian to polar transformation in order to select a region to be removed. Firsty, in polar coordinates, the atoms that were not in the region within the clearance angle (α) and the rake angle (γ) were removed. Second, an inverse transformation from polar to cartesian was performed, and the tool origin was translated to O' (Figure *1 (c)*). Finally, once again in polar coordinates, the cutting edge was rounded, by removing atoms with angle coordinates within the interval [(180º+ γ), (270º+ α)], but with radius coordinate bigger than the tool radius (Figure *1 (d)*). To avoid approximation errors during the Cartesian to polar transformation and back, instead of removing the atoms coordinates directly, the operations just selected indexes to be either kept or removed. In other words, a mask was built for the atom's coordinates matrix.
Another characteristic for discussion is the effective rake angle (γ_{eff}), that was defined as the angle (AEC), formed by the tangent AI and the vertical reference line Y'', as represented in Figure 2. The tangent AI is defined as the tangent on the middle of angle DO'F, formed by the cutting edge.

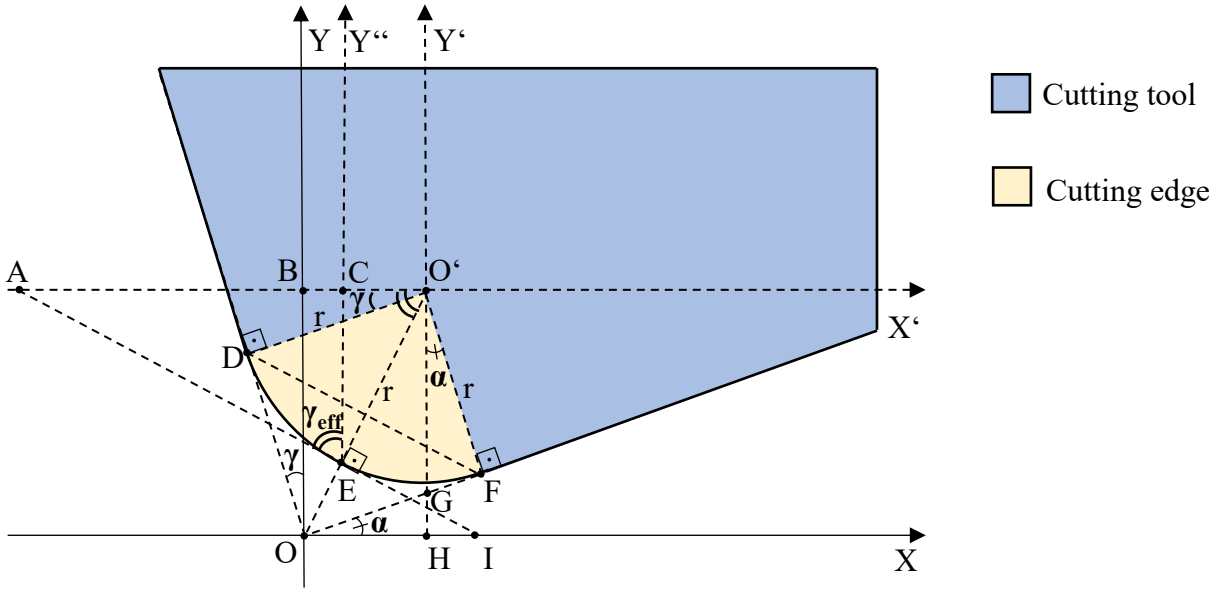

Figure 2 – Effective rake angle.

Based on the definition, on the angles that match α and γ on Figure 2 model, and on the fact that the angle DO'O is half of the angle DO'F, γ_{eff} was calculated as follows:

$$\gamma_{eff} = (90 + \alpha - \gamma)/2 \qquad \text{Eq. (1)}$$

Based on the Equation-1, the value of γ_{eff} is not a function of tool radius (r). However, the smaller the value of r, the faster is the transition from γ to γ_{eff}. Thefore the following relation is defined:

$$K_{\gamma} = (\gamma_{eff} - \gamma)/r \qquad \text{Eq. (2)}$$

Where K_{γ} is a measure of the change on γ due to the r. The bigger the value of K, the more abrupt is the transition from γ to γ_{eff}.
Since molecular models are discrete and not continuous representations of the matter, Equation-2 may failure to address how abrupt or smooth the γ to γ_{eff} might be. Therefore, a more generalized equation form is presented as follows:

$$K_{\gamma} = \frac{\widehat{DE}}{r^2} \qquad \text{Eq. (3)}$$

In a tool model for CMDS, the arc $\widehat{DE}$ can be shorter than in representation shown in Figure 2 if the radius is not big enough. On the other hand, since the angle DO'E is numerically equal to the difference between γ and γ_{eff}, for bigger values of r and γ and γ_{eff} values are in radians, Equation-3 and Equation-2 are equivalent.

3. METHODOLOGY

3.1 Potential

For GaP and for carbon, a Vashishta potential parametrized by Picini *et al.* [26], and a SiC Tersoff force field available at LAMMPS were used respectively. For interaction between tool and workpiece, Lenard-Jones potential was applied.
The potential used to GaP was previously tested for nanoindentation, successfully showing the gallium Phosphide HPPT [27]. It was shown that even in presence of shear stress, the gallium phosphide changes from zincblende to β-tin under hydrostatic pressures above 15,3 GPa.

3.2 Model and simulation

Two different simulations were performed with two different rake angles (-20 and -10), 12 nm cutting thickness, 10 nm tool edge radius, and cutting speed was 1200 m/min (0.2 Å/ps). The model used for the cutting mechanism simulation is represented in the Figure 3.

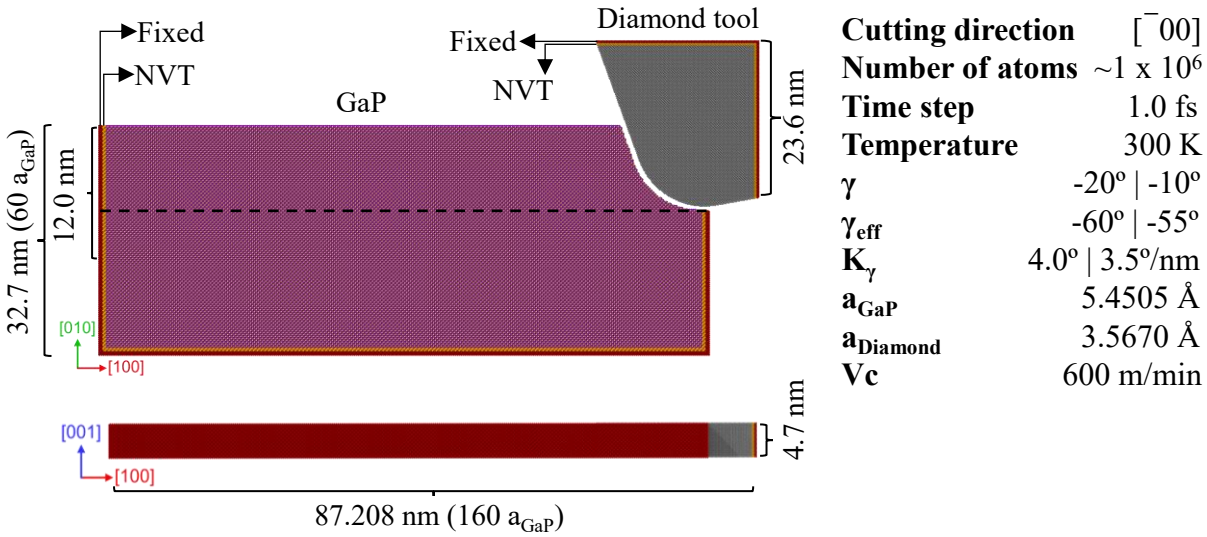

Figure 3 – Model for cutting mechanism simulation considering the tool contact.

Differently from the literature [9,23,28], in the present model, the workpiece has a chamfer with a fillet that matches the tool cutting edge shape. This was intended to minimize efforts of the first contact tool-workpiece and to allow the contact both cutting edge and tool face at the same time. Both tool and workpiece have three layers:

- **NVT layer (Canonical Ensemble):** Since the model has a limited number of atoms, it requires a method to mimic the heat-absorbing capacity of a much larger body. In other words, the system needs to be immersed in a heat bath. For this purpose, the Nosé-Hoover thermostat algorithm, commonly used in CMDS, was applied. This algorithm maintains a constant temperature (T) by periodically resetting it to a predetermined value (e.g., 300 K) during interactions, while keeping the average temperature, simulation box volume (V), and number of atoms (N) constant.
- **NVE layer (Microcanonical Ensemble):** In this layer, the system was allowed to change its temperature while keeping the number of atoms and volume constant throughout the simulation.
- **Fixed Atoms layer:** This group of atoms is treated as an NVE ensemble, but the forces acting on the system are set to zero for the entire duration of the simulation. This arrangement enables this group of atoms to remain stationary and avoids the overall system collapse.

The simulation also has computational and numerical related parameters such as:

- **Number of processors:** 20 for the simulation with $\gamma = -20^{o}$ and 100 for $\gamma = -10^{o}$. In both cases, the process grid was number of processors x 1 x 1, meaning that the simulation was only split along the cutting direction.
- **Neighbour list update rate:** every 5 timesteps for the simulation with $\gamma = -20^{o}$ and every 10 for $\gamma = -10^{o}$. Since the tool does not visually moves even for 500 timesteps, the update rate was increased one the second simulation.
- **Boundary:** periodic in [001] direction and resizable in the other two.
- **Total number of time steps:** 1.5 million, which represents 1.5 nanoseconds.
- **Equilibration:** the system kept at 300 K for 2000 timesteps before the start of the simulations for $\gamma = -20^{o}$. For $\gamma = -10^{o}$, the simulation were performed a second time due to an excessive energetic single atom that scape from the process. Without dissipative forces, this atom moved indefinitely, stretching the simulation cell in both shrinkable directions, to the point more than half of the simulation cell was filled with a single atom using 50 processors to calculate its trajectory. The simulation was interrupted, and the equilibration time was increased ten times, solving the problem.
- **Frame save rate:** every 10 000-timesteps and every 500 during the hydrostatic pressure calculation region.

3.3 Post processing

The post processing was fundamentally focus on the analysis of the phase transformations of the GaP workpiece. Therefore, it was first necessary to calculate the hydrostatic pressure of the system.

3.3.1 Hydrostatic pressure

Since the hydrostatic pressure is a value from the continuous mechanics and not from the atomistic scale, it was necessary a conversion as follows:

$$\sigma_{abi} = \frac{S_{abi}}{V_i} \qquad \text{Eq. (4)}$$

Where σ_{abi} is Cauchy tensor, S_{abi} the virial stress as calculated by LAMMPS, and V_i is the atomic volume for every i-atom, while a and b can assume the x, y, and z components.
To calculate the Cauchy tensor in this way it is also necessary to average the value in time and space. For spatial averages, a 5.4505 Å shell was used around every atom to define a set of atoms. For time averages, ten frames evenly spaced with 500 timesteps were used. That means the frame save rate of the simulation was increase for a moment (between 500 000- and 600 000-time steps), just to allow the Cauchy stress tensor calculation.
Finally, the hydrostatic pressure (p) calculation was performed as normal, through the polar decomposition of the Cauchy tensor as follows:

$$p = \frac{-\mathrm{tr}(\boldsymbol{\sigma})}{3} \qquad \text{Eq. (5)}$$

Where $\mathrm{tr}(\boldsymbol{\sigma})$ is the trace of the Cauchy tensor (sum of the diagonal terms for second order tensors).

3.3.2 Structure identification

For the structure identification, two different algorithms were used: Dislocation Extraction Analysis (DXA) and Polyhedron Template Matching (PTM), both available in the Ovito® software. DXA is also capable of calculate the dislocations, which means it was used even when PTM was more accurate. In the Figure 4 the structure identification methodology is presented.

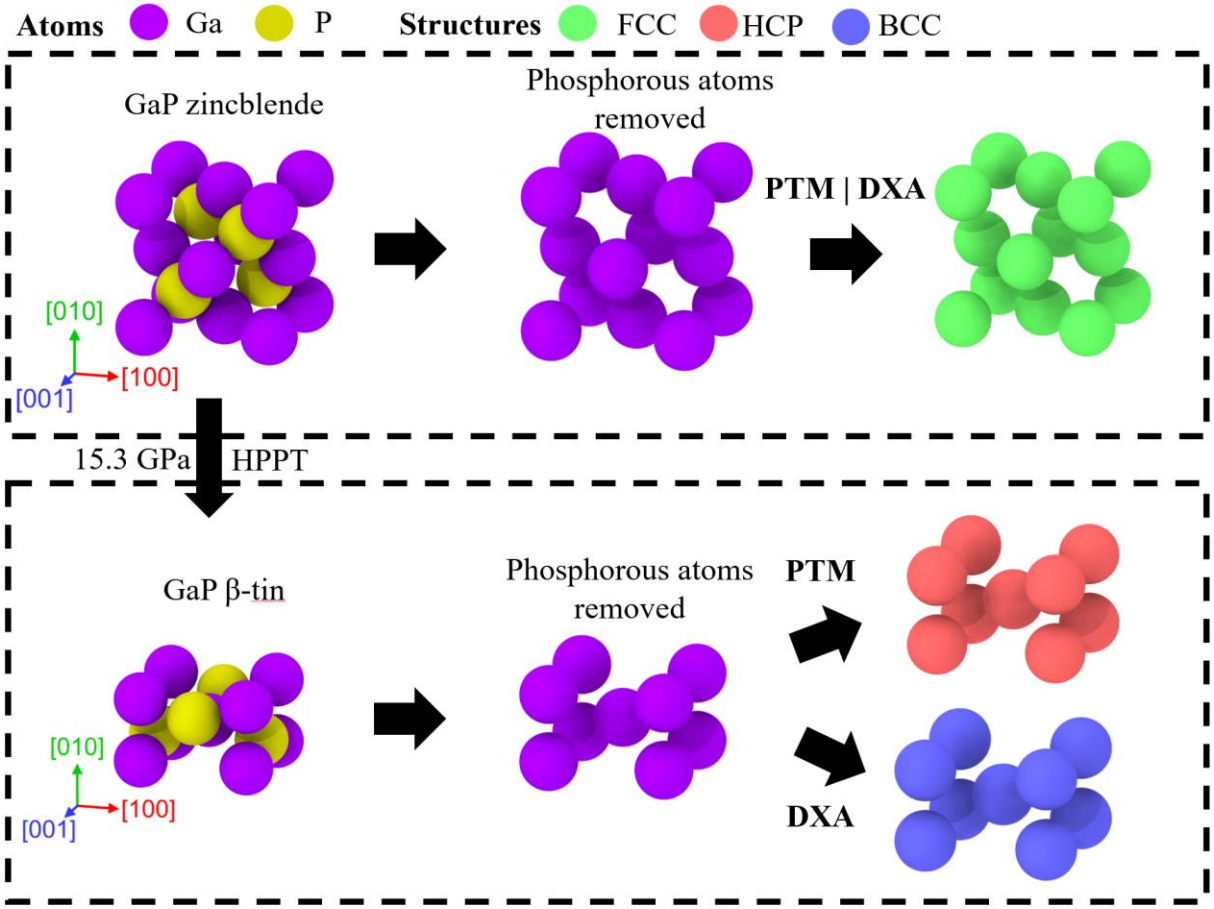

Figure 4 – Structure identification methodology using algorithms available on Ovito®.

The β-tin structure is not directly available to either DXA or PTM, therefore, the phosphorous atoms were hidden, so both algorithms were able to identify it as some structure. The DXA reads the β-tin as a BCC structure, but it needs a considerable number of lattices, otherwise it does not identify any structure (it outputs the value "other"). The PTM identifies β-tin as HCP, but this structure is also related to stack fault in FCC structures. Meaning PTM has the same output for two different phenomena. Since none of the algorithms were capable of isolate the structure, the results were compared with the hydrostatic pressure.

3.3.3 Radial distribution function (RDF)

Radial distribution function (RDF) can be applied to measure the possibility to find one specific bond length within a simulation cell. They are normalized by the cell volume. In CMDS it is possible to evaluate the amorphization and graphitization of the diamond when they happened [9]. The former wear mechanism happens when the base of the peaks in a RDF curve enlarges, meaning more bond lengths can be found. The latter is identifiable by an increasing on bond with length 1.42 Å, which corresponds to carbon-graphite bond length [23].

3.3.4 General considerations for results representation

For simplicity the NVT and fixed atoms were removed from simulation results representations. The procedure of removing the phosphorus atoms in post-process stage (except for hydrostatic pressure calculation) reduced the time required to analyze the simulation. Therefore, most of the results are shown without phosphorus atoms as well.
The algorithm used to calculate the hydrostatic pressure was computational expensive, so only one frame was used. Additionally, the carbon atoms from the diamond tool were removed for the calculation. Future versions of the algorithm with parallel processing capabilities, might solve the problem.

4. RESULTS AND DISCUSSION

4.1 Results for rake angle -10º

In Figure 5 it is possible to see the fracture during the cut (Figure 5 (a) and (d)), the hydrostatic pressure (Figure 5 (c)) and the variation of the tool bond length during the simulation Figure 5 (d).

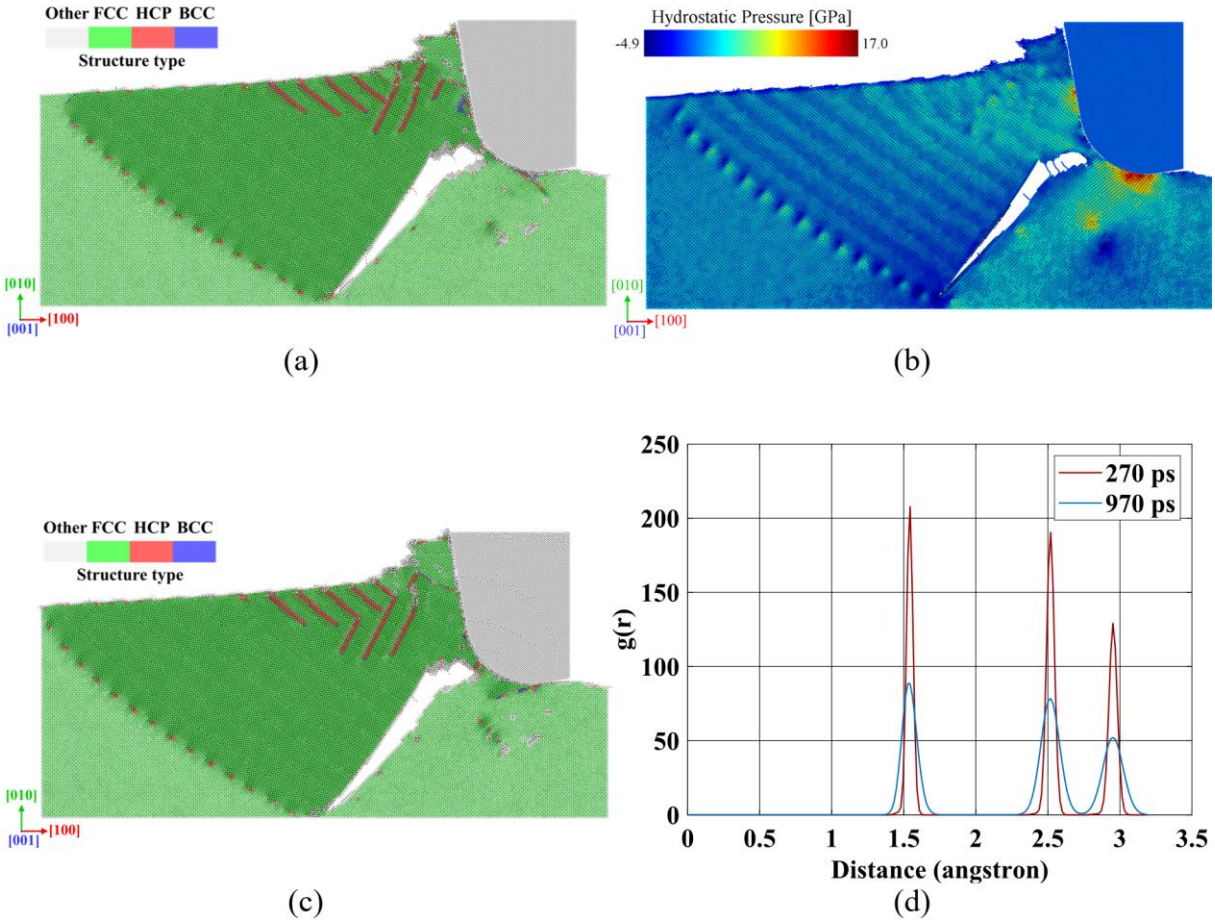

Figure 5 – Simulations with rake angle equal to -10º: (a) simulation frame post processes at 500 ps by hiding phosphorous atoms and applying PTM algorithm, (b) hydrostatic pressure at 500 ps, (c) same as (a), but for 970 ps, and (d) radial distribution function between the 270 and 970 ps (interval with the same simulation box).

The atoms in HCP structure (red atoms) represent stacking faults, a planar movement of dislocations along planes $\{11\bar{1}\}$ and $\{111\}$ for the FCC, zincblende, and cubic diamond lattices. This mechanism represents the shear of the GaP and it is desirable if it happens on the planes

{111}. The presence of stack faults on the direction {11$\bar{2}$} represents an undesirable mechanism, that forces the movement of atoms towards the tool face instead of towards the cutting direction [29].
Stacking faults dislocation requires a linear dislocation moving along the crystal in a direction 90º in relation to the movement of the planar one [29]. Consequently, the cutting direction should have a component parallel to this linear dislocation. However, when the γ_{eff} = 45º, this component reaches its minimum, while the component normal to the stacking fault reaches its maximum, favouring the crack formations as the one represented in Figure 5. This is a consequence of the discrete nature of the diamond crystal that allows a tool effective rake angle of 45º instead of the calculated 55º. Moreover, the transition was not smooth, rather abrupt (greater K_γ), and this angle exists not in as ideal point, but along of a plane. A 45º plane with small area is on the cutting edge, reducing the pressure applied close to it (Figure 5 (b)), creating a small stagnation zone that moves with the tool.
The hydrostatic pressure reached values above 15.3 GPa, pressure required for the zincblende-β-tin HPPT to happen, but only in a small on the tool face and under the tool, on the beginning of the flank face. This and the shear motivated by the stacking faults, indicate that the HPPT is not the main cutting mechanism, but a phenomenon that might smooth the machined surface after the cutting. Simulation with bigger tool radius would be helpful to analyse how far can this HPPT zone be, if can be a cutting mechanism and if can minimize the crack formation.
The radial distribution function for the tool (Figure 5(d)) started on 270 ps instead of on 0 ps due the shrink of the simulation cell on the beginning of the tool movement. RDF uses the simulation cell volume to normalize the output data, so the comparison within the same simulation cell size avoids misleading conclusions. From 270 to 970 ps, the simulation cell remained the same. It is possible to observe a variation on atomic distances along the simulation. This should be an effect of cutting process efforts, but the peaks on 2.55 and 2,95 seems to merge in the end of the simulation. This is a sign of amorphization of the tool.

4.2 Rake angle -20º

The results for a rake angle γ = -20º shows a far smaller crack as can be seen in Figure 6 (a), (b), and (c). The hydrostatic pressure reaches 15.3 GPa (Figure 6(b)), the minimum required for GaP to change its phase from zincblende to β-tin based on the force field used. Through the RDF, it is possible to observe that the tool suffers less stress, since the peaks are far to merge in one, remaining very defined even after the simulation (Figure 6(d)).
The calculated effective rake angle was -60º, but once more, due to the discreate nature of the cubic diamond structure, the effective rake angle was 45º. The K_γ is still smaller the for γ = -10º, meaning a smaller transition. Regardless of that, a small plane was also present on the tool cutting edge, and a stagnation region appears in front of the cutting edge followed by a crack.
The stacking fault defects were formed towards the cutting direction. No dislocation plane moved towards the tool face, meaning the cutting process is more likely to lead to a better surface quality than for the cutting with γ = -10º.
Once again, the pressure necessary for a HPPT happened only in a small portion of the simulation on the deformation zone. Additionally, for both simulations, the hydrostatic pressure increases 45º bellow the cutting edge reaching the bottom of the simulation cell. This emulates a material harder expected indicating that higher workpiece would be preferable for future works.

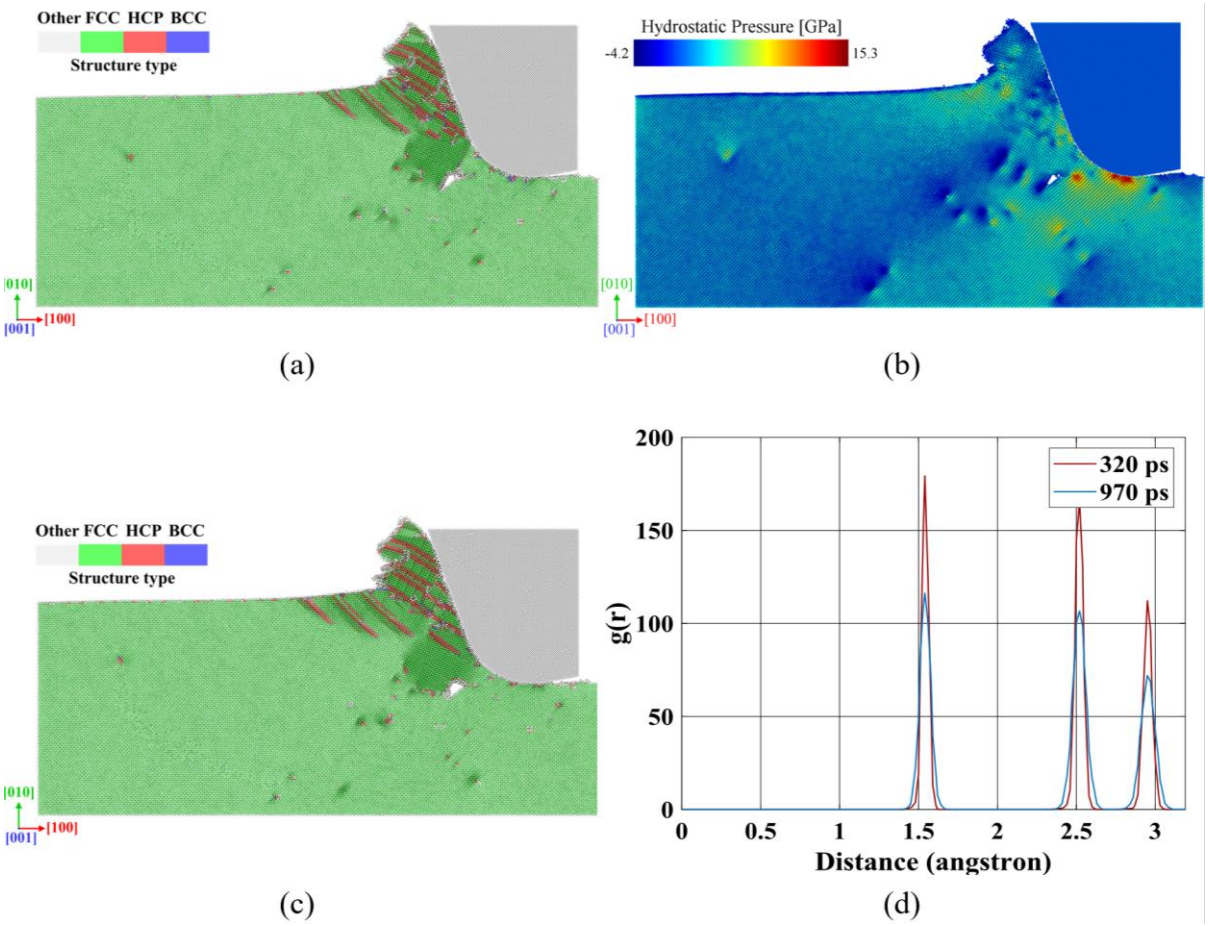

Figure 6 - Simulations with rake angle equal to -20°: (a) simulation frame post processes at 500 ps by hiding phosphorous atoms and applying PTM algorithm, (b) hydrostatic pressure at 500 ps, (c) same as (a), but for 970 ps, and (d) radial distribution function between the 320 and 970 ps (interval with the same simulation box).

5. CONCLUSIONS

GaP cutting mechanism simulations were performed using classic molecular dynamics for two different rake angles. The following findings were observed analyzing simulations results:

- The main cutting mechanism was stacking faults, a planar defect characterized by the movement of a layer of atoms breaking the stacking sequence of a crystal. When this movement does not push atoms against the tool face, crack formation was less significative.
- Due the discrete nature of a crystal, stagnation zones were present in both simulations close to the cutting edge. Since cracks were formed in front of them, there seems to exist a relation between the two.
- The HPPT appeared only in the deformation zone, meaning it might not be a cutting mechanism.
- Finally, the beginning of an amorphization was detect on the tool for $\gamma = -10^{\circ}$ with the aid of RDF.

6. OUTLOOK

Future studies can use different force fields for the diamond tool in GaP cutting mechanism simulations, with a focus on investigating if other types of tool wear can be simulated. Another possibility is conduct simulations with a tool edge radius larger than 10 nm to ensure a smoother

transition between the rake angle and the effective rake angle, thus improving the modelling accuracy. Additionally, a higher workpiece height might prevent material hardening caused by the propagation of hydrostatic pressure.

7. ACKNOWLEDGEMENTS

This project was possible due to the contribution from National Council for Scientific and Technological Development from Brazil (CNPQ).

REFERENCES

[1] Václavík J, Vápenka D. Gallium Phosphide as a Material for Visible and Infrared Optics. EPJ Web Conf 2013;00028:1–4. https://doi.org/10.1051/epjconf/20134800028.
[2] Vaclavík J, Doleček R, Lédl V, Psota P. Experimental Study on SPDT Machining of Gallium Phosphide. Proceedings of Spie 8884, New York: 2013. https://doi.org/10.1117/12.2036139.
[3] Rivoire K, Lin Z, Hatami F, Ted Masselink W, Vučković J. Second harmonic generation in gallium phosphide photonic crystal nanocavities with ultralow CW pump power. Optics InfoBase Conference Papers 2010;17:22609–15. https://doi.org/10.1364/qels.2010.qwe4.
[4] Arata I, Kobayashi M, Matsuda S, Terada H. Evaluation of Gallium Phosphide Substrate for Solid Immersion Lens. n.d.
[5] Kühne S, Jagodzinski M, Polte J, Scholz P, Uhlmann E. Ultra-precision machined gallium phosphide solid immersion micro lenses for aperture magnification in measurement systems (oral presentation). 2016.
[6] Uhlmann E, Oberschmidt D, Rolon DA, Kühne S, Jagodzinski M, Malcher M. Ductile machining of brittle materials for manufacturing micro-optic components. 2018.
[7] Arrazola PJ, Özel T, Umbrello D, Davies M, Jawahir IS. Recent Advances in Modelling of Metal Machining Processes. CIRP Ann Manuf Technol 2013;62:695–718. https://doi.org/10.1016/j.cirp.2013.05.006.
[8] Chandrasekaran H, M'saoubi R, Chazal H. Machine Science and Technology Modelling of material flow stress in chip formation process from orthogonal milling and split Hopkinson bar tests. Machine Science and Technology 2005;9:131–45. https://doi.org/10.1081/MST-200051380.
[9] Goel S, Luo X, Agrawal A, Reuben RL. Diamond Machining of Silicon: A Review of Advances in Molecular Dynamics Simulation. Int J Mach Tools Manuf 2015;88:131–64. https://doi.org/10.1016/j.ijmachtools.2014.09.013.
[10] Marinescu ID, Rowe WB, Dimitrov B, Ohmori H. Tribology of Abrasive Machining Processes. 2th ed. Oxford: William Andrew Publishing; 2013. https://doi.org/https://doi.org/10.1016/B978-1-4377-3467-6.00001-X.
[11] Cai W, Li J, Yip S. Molecular dynamics. Comprehensive Nuclear Materials 2012;1:249–65. https://doi.org/10.1016/B978-0-08-056033-5.00128-2.
[12] Voyiadjis GZ, Yaghoobi M. Molecular dynamics. Size Effects in Plasticity 2019:275–355. https://doi.org/10.1016/b978-0-12-812236-5.00005-0.
[13] Ribeiro-Silva CI, Picinin A, Rino JP, Menezes MG, Capaz RB. Temperature effects on the structural phase transitions of gallium phosphide. Comput Mater Sci 2019;161:265–75. https://doi.org/10.1016/j.commatsci.2019.02.010.
[14] Sandia Corporation. Neigh_modify command. Https://DocsLammpsOrg/Neigh_modifyHtml 2023.

[15] Stukowski A. Dislocation Analysis Tool for Atomistic Simulations 2018:1–14.
[16] Stukowski A, Bulatov V V., Arsenlis A. Automated identification and indexing of dislocations in crystal interfaces. Model Simul Mat Sci Eng 2012;20. https://doi.org/10.1088/0965-0393/20/8/085007.
[17] Stukowski A, Albe K. Extracting dislocations and non-dislocation crystal defects from atomistic simulation data. Model Simul Mat Sci Eng 2010;18. https://doi.org/10.1088/0965-0393/18/8/085001.
[18] Larsen PM, Schmidt Sø, SchiØtz J. Robust structural identification via polyhedral template matching. Model Simul Mat Sci Eng 2016;24. https://doi.org/10.1088/0965-0393/24/5/055007.
[19] Jiapeng S, Cheng L, Han J, Ma A, Fang L. Nanoindentation Induced Deformation and Pop-in Events in a Silicon Crystal: Molecular Dynamics Simulation and Experiment. Sci Rep 2017;7:1–12. https://doi.org/10.1038/s41598-017-11130-2.
[20] Subramaniyan AK, Sun CT. Continuum Interpretation of Virial Stress in Molecular Simulations. Int J Solids Struct 2008;45:4340–6. https://doi.org/10.1016/j.ijsolstr.2008.03.016.
[21] Belak JF, Stowers IF. A molecular dynamics model of the orthogonal cutting process, United States: 1990.
[22] Komanduri R, Raff LM. A Review on the Molecular Dynamics Simulation of Machining at the Atomic Scale. Journal of Engineering Manufacture 2001. https://doi.org/10.1177/095440540121501201.
[23] Goel S, Luo X, Reuben RL. Molecular Dynamics Simulation Model for the Quantitative Assessment of Tool Wear During Single Point Diamond Turning of Cubic Silicon Carbide. Comput Mater Sci 2011;51:402–8. https://doi.org/10.1016/j.commatsci.2011.07.052.
[24] Maekawa K, Itoh A. Friction and Tool Wear in Nano-Scale Machining: a Molecular Dynamics Approach. Wear 1995;188:115–22.
[25] Sharma A, Datta D, Balasubramaniam R. A Molecular Dynamics Simulation of Wear Mechanism of Diamond Tool in Nanoscale Cutting of Copper Beryllium. International Journal of Advanced Manufacturing Technology 2019:731–45.
[26] Ribeiro-Silva CI, Rino JP, Gonçalves LG V, Picinin A. An effective interaction potential for gallium phosphide. Journal of Physics: Condensed Matter 2011;23:055801. https://doi.org/10.1088/0953-8984/23/5/055801.
[27] Tavares MRPM, Rolon DA, Kober J, Misturini A, Kühne S, Schroeter RB, et al. Analysis of gallium phosphide phase transformations under nanoindentation with the aid of molecular dynamics simulations. In: euspen, editor., Copenhagen: Proceeding Engineering; n.d.
[28] Zongxiao ZHU, Bin P, Ruicheng F, Linjun W, Shi J, Yun D. Molecular Dynamics Simulation of Chip Formation Mechanism in Single-Crystal Nickel Nanomachining 2019;62:1916–29.
[29] Hull D, Bacon DJ. Chapter 1 - Defects in Crystals. In: Hull D, Bacon DJ, editors. Introduction to Dislocations (Fifth Edition). Fifth Edition, Oxford: Butterworth-Heinemann; 2011, p. 1–20. https://doi.org/https://doi.org/10.1016/B978-0-08-096672-4.00001-3.

CONTACTS

M.Sc. Michel R. P. M. Tavares
email: tavares@mfg.tu-berlin.de
ORCID: https://orcid.org/0000-0002-0070-3633

